haematologica
Journal of the Ferrata Storti Foundation

T-cell receptor architecture and clonal tiding provide insight into the transformation trajectory of peripheral T-cell lymphomas

by Edith Willscher, Christoph Schultheiß, Lisa Paschold, Franziska Lea Schümann, Paul Schmidt-Barbo, Benjamin Thiele, Marcus Bauer, Claudia Wickenhauser, Thomas Weber, and Mascha Binder

Received: March 1, 2024.
Accepted: August 22, 2024.

Citation: Edith Willscher, Christoph Schultheiß, Lisa Paschold, Franziska Lea Schümann, Paul Schmidt-Barbo, Benjamin Thiele, Marcus Bauer, Claudia Wickenhauser, Thomas Weber, and Mascha Binder. T-cell receptor architecture and clonal tiding provide insight into the transformation trajectory of peripheral T-cell lymphomas.
Haematologica. 2024 Aug 29. doi: 10.3324/haematol.2024.285395 [Epub ahead of print]

T-cell receptor architecture and clonal tiding provide insight into the transformation trajectory of peripheral T-cell lymphomas

*Edith Willscher[1], *Christoph Schultheiß[2,3], Lisa Paschold[1], Franziska Lea Schümann[1], Paul Schmidt-Barbo[2], Benjamin Thiele[2,3], Marcus Bauer[4], Claudia Wickenhauser[4], Thomas Weber[1], Mascha Binder[2,3]

[1] Internal Medicine IV, Oncology/Hematology, Martin-Luther-University Halle-Wittenberg, Halle, Germany

[2] Department of Biomedicine, Translational Immuno-Oncology, University of Basel, Basel, Switzerland

[3] Division of Medical Oncology, University Hospital Basel, Basel, Switzerland

[4] Department of Pathology, Martin-Luther-University Halle-Wittenberg, Halle, Germany

* These authors contributed equally

Author contributions

EW and CS contributed equally as co-first authors.

Idea & design of research project: MB, TW; Supply of critical material (e.g. patient material, cohorts): TW, CW, FLS; Experimental work: CS, LP, MBa; Dataanalysis and –interpretation: EW, MB, CS, BT, LP, PSB, TW; Drafting of manuscript: MB, EW, BT

Running heads

Clonal tiding in T cell lymphomas

Corresponding author

Mascha Binder, mascha.binder@usb.ch

Data-sharing statement

The TCR sequencing data reported in this article have been deposited at European Nucleotide Archive (ENA) at EMBL-EBI under accession number PRJEB72787.

Word count: Abstract 177 words; main text 3.157 words; five figures and one table are present in the manuscript; one supplementary file

Acknowledgements

The authors thank A. Patzschke as well as Alexander Navarrete-Santos and the UKH Core Facility Flow Cytometry for excellent technical assistance.

Funding

Deutsche Krebshilfe (70114663 to M.B.), OSHO (OSHO#93 to T.W.)

Disclosures

The authors disclose no potential conflicts of interest.

Abstract

While T cell lymphomas are classified as mature neoplasms, emerging evidence indicates that malignant transformation may occur at an earlier stage of T cell maturation. In this study, we determined clonal architectures in a broad range of T cell lymphomas. Our multidimensional profiling indicates that a large part of these lymphomas in fact emerge from an immature lymphoid T cell precursor at a maturation stage prior to V(D)J rearrangement that undergoes branching evolution. Consequently, at single cell resolution we observed considerable clonal tiding under selective therapeutic pressure. T cell receptor next-generation sequencing suggested a highly biased usage of TRBV20-1 gene segments as part of multiple antigen receptor rearrangements per patient. The predominance of TRBV20-1 was found across all major T cell lymphoma subtypes analyzed. This suggested that this particular V gene – independently of complementarity-determining region 3 (CDR3) configuration - may represent a driver of malignant transformation. Together, our data indicate that T cell lymphomas derive from immature lymphoid precursors and display considerable intratumoral heterogeneity that may provide the basis for relapse and resistance in these hard-to-treat cancers.

Introduction

T cell lymphomas are a heterogenous group of malignancies that may reside in lymph nodes, other primary or secondary lymphoid organs or even extralymphatic sites.[1-7] Treatment for this group of diseases is systemic and includes chemotherapy, antibody-drug conjugates as well as stem cell transplantation.[3,8,9] Yet, the prognosis remains poor. Especially after failure of first-line treatment only up to 25% of patients experience long-term survival.[10-13] There is an unmet clinical need to better understand the biological underpinnings of this group of diseases to establish novel avenues for precision targeting.

T cell lymphomas are classified as mature neoplasms due to their immunophenotype that closely resembles subsets of normal mature T cells and their rearranged T cell receptor (TCR) V(D)J genes.[14-17] The TCR rearrangement is an excellent maturation marker since TCRγ, TCRβ, and TCRα loci are sequentially rearranged from a diverse pool of V(D)J genes during various stages of intrathymic development.[18] As a result, each naive T cell that emigrates from the thymus has a unique TCR gene rearrangement that is retained as the cell divides and differentiates. Prior to the development of advanced technical methods for TCR clonality analysis, the prevailing theory was that T cell lymphomas are clonal diseases that originate from a single mature T cell that has undergone both positive and negative selection within the thymus.[19] However, recent advancements in sequencing have revealed that several types of T cell lymphomas are in fact oligoclonal in nature, indicating that they originate from multiple clones with distinct TCR rearrangements, rather than a single clone.[14] This challenges the “maturity” paradigm in lymphoma development and points to a lymphoid precursor as cell of origin. In angioimmunoblastic T cell lymphoma (AITL) – one of the major subtypes of T cell lymphomas and characterized by a T follicular helper (T_{FH}) phenotype[20,21] – there is additional evidence supporting this view. In this particular subtype, branching evolution appears to start as early as at the level of the hematopoietic stem cell.[22] The genetic landscape of AITL suggests that the initial

oncogenic event might consist in mutations that are typically found in clonal hematopoiesis such as *TET2* or *DNMT3A.*[20,23] These mutant hematopoietic stem cell (HSC) may then have the potential to evolve to AITL as well as neoplasms of other hematopoietic lineages.[24,25] This may also explain the frequent coexistence of lymphoid and myeloid cancers in patients with AITL.[26] For other T cell lymphomas, the transformation trajectory including the acquisition of driver mutations is much more ill-defined.[27,28]

Here, we determined clonal architectures in a broad range of T cell lymphomas and their development with or without selective therapeutic pressure to gain insight into the mechanism of treatment failure for this hard-to-treat cancer.

Methods

Methods are provided more detailed in the *Online Supplementary Appendix*.

Patient samples and tissue microarray

Lymphoma tissue was collected after informed consent as approved by the ethics committee of the University of Halle-Wittenberg (number 2021-074 and 2020-033). Distribution of cases and samples are shown in Table 1 and *Online Supplementary Table 1*.

T cell receptor (TCR) immune repertoire sequencing and data analysis

The V(D)J rearranged TRB loci were amplified from genomic DNA isolated from formalin-fixed and paraffin embedded (FFPE) tissue and sequenced on an Illumina MiSeq (Illumina, San Diego, USA) with a 601-cycle paired-end run and V3-chemistry as described in Schultheiss et al[29] and Simnica et al[30,31] The MiXCR framework[32] v.3.0.12 was used for sequence alignment and clonotype (considered as one uniqe nucleotide CDR3 sequence) assignment. Non-productive reads and clonotypes with less than 2 reads were discarded.

TCR repertoires from patients with acute COVID-19 infection were derived from Schultheiß et al[33] For analysis of repertoire metrics, healthy immune repertoires were proportionally normalized to 30,000 productive reads. A more detailed description of immune repertoire data generation, processing and analyses is given in the *Online Supplementary Appendix*.

Tissue microarray staining for TRBV20-1 usage

Available FFPE tissue from our TCR-NGS cohort as well as additional T cell lymphoma samples were analyzed using a tissue microarray as reported by Schümann et al[34]. The staining was performed on 3 µm tissue sections using the TCR Vβ2-PE antibody (diluted 1:100, IM2213, Beckmann Coulter, CA).[35-37] Deparaffinization and peroxidase block was performed as described in Bauer et al[38].

Gene panel profiling

Profiled hotspots mutations associated with T cell lymphomas are listed in Supplementary Table 2. Sequencing libraries were constructed using Qiaseq Targeted DNA Custom Panels (Qiagen, Hilden, Germany) and sequenced on a Illumina NextSeq 500 platform with 2 x 150 cycles at an average coverage of 52,700 reads per target region. Variant calling of unique molecular identifier (UMI) was performed using CLC Workbench (Quiagen). Mutations were considered as positive if they were found with a variant allele frequency (VAF) exceeding 10% at a read depth of more than 70 reads. To filter for disease relevant mutations, common single nucleodtide polymorphisms (SNPs) stated by dbSNP were discarded as well as synonymous variants.

Cell sorting and single-cell transcriptomic profiling

To enrich lymphoma cells for single-cell analyses using the 10X Genomics platform, we sorted the malignant cells of a T-PLL case based on their aberrant CD4+/CD8+

immunophenotype and cells of an AITL case for aberrant CD3 surface expression from cryopreserved peripheral blood mononuclear cells (PBMCs) using the anti-CD3-APC-H7 (clone SK7, BD Biosciences), anti-CD4-PacificBlue (clone RPA-T4, Biolegend) and the anti-CD8-FITC (clone SK1, BD Biosciences) antibodies. Sequencing, data processing and analysis was performed as described by Schultheiß et al[39].

Results

TCR profiling of T cell lymphomas shows marked oligoclonality and overrepresentation of TRBV20-1 rearrangements

We studied T cell lymphoma tissue (Table 1, TCR-NGS subcohort; *Online Supplementary Table 1*) by next-generation TCR sequencing to obtain insight into TCR clonality and gene usage of these cases. Most of these patients had angioimmunoblastic T cell lymphomas (AITL) or peripheral T cell lymphomas not otherwise specified (PTCL NOS). As a reference for TCR metrics, we used blood from 121 healthy individuals.

In order to avoid bias, we utilized only one sample per patient (baseline or earliest available time point) to study the broad TCR architecture across this range of lymphomas. In general, T cell lymphomas showed higher TCR clonality as compared to blood of healthy individuals (Figure 1A). To visualize TCR gene usage in the repertoire, we plotted the frequency of unique V, D and J gene rearrangements on a V(D)J matrix for one healthy sample and an oligoclonal- and monoclonal T-NHL case (Figure 1B). We classified each case as oligo- or monoclonal based on the algorithm described in the methods section taking into account the tumor cell infiltration of each case and the statistical frequency of biallelic rearrangements. According to this definition, 47.4% of cases were oligoclonal, while 52.6% were monoclonal (Figure 1C). Next, we performed principal component analysis (PCA) to investigate V or VJ gene skewing of the lymphoma TCR repertoire towards specific receptor rearrangements. This analysis revealed a substantial skewing of

lymphoma repertoires (Figure 1D). TRBV20-1 was the V gene contributing most to this skewing (Figure 1D, right side; *Online Supplementary Figure 1*). Yet, as shown in the exemplary case from panel 1B, heterogeneous rearrangements were present without evidence for a specific complementarity-determining region 3 (CDR3) sequence involved. To compare the usage of TRBV20-1, we used blood-derived T cells from healthy donors and patients with acute COVID-19 as control. The COVID-19 samples were derived from an own previously published dataset[33] and were chosen due to the high systemic inflammatory dysregulation (e. g. excessive IL6, TNF) during acute infection which was linked to TRBV20-1 expansion in some cases[40]. This analysis showed a median TRBV20-1 usage of around 1% in the controls, while the median TRBV20-1 usage was around 40% in T cell lymphomas (Figure 1E). When examining TCR architecture in samples obtained at the initial diagnosis and those collected at disease progression, we did not observe changes in TCR repertoire metrics within our specific cohort size (Figure 1F). Also, TCR repertoire metrics were very similar in different lymphoma subtypes as shown for AITL and PTCL NOS in *Online Supplementary Figure 2*.

Tissue microarray staining confirms preferential usage of TRBV20-1 in the majority of cases

To confirm this striking overrepresentation of TRBV20-1 rearrangements in lymphoma tissue of T cell lymphoma patients, we subjected T cell lymphoma cases including the majority of the TCR-NGS subcohort (Table 1) to TRBV20-1 staining using a monoclonal commercial antibody (Figure 2A). The samples of this cohort were distributed across three tissue microarrays. Consistently with our NGS results, the majority of samples showed some positivity for TRBV20-1 in the lymphoma tissue (exemplarily shown in Figure 2A). While only very few cases were homogeneously positive for TRBV20-1 throughout the tissue section (Figure 2, exemplarily shown in a), many samples showed a patchy

distribution of TRBV20-1 signals (Figure 2, exemplarily shown in b) suggesting that TRBV20-1 rearrangements were expressed along with other rearrangements in the lymphoma. About 50% of samples showed no staining for TRBV20-1 at all (Figure 2, exemplarily shown in c). Matching of NGS and tissue microarray staining data showed concordant results in some cases, but not in all, speaking in favor of spatial intratumoral heterogeneity. Of the four cases with strong and homogeneous positivity for TRBV20-1 on Immunohistochemistry, three showed very high TRBV20-1 gene usages taking up between 87.5 and 100% of the malignant repertoire. Samples with heterogeneous or negative staining results showed variable levels of TRBV20-1 usage (Figure 2B). In the largest lymphoma entities of this cohort – AITL, PTCL NOS and anaplastic large cell lymphoma (ALCL) – TRBV20-1-containing rearrangements were about equally prevalent (Figure 2B right panel).

Genetic heterogeneity extends to alpha chain rearrangements and corresponds with transcriptomic heterogeneity

To better understand genetic and transcriptomic heterogeneity at single-cell resolution, we performed TCR and single-cell RNA sequencing on enriched lymphoma cells from two patients, patient 055 with T prolymphocytic leukemia (T-PLL) and patient 056 with AITL.

The integration of these lymphoma cells with T cells of two healthy individuals retrieved from Herrera et al[41] (sample HC1) and resource datasets from 10X Genomics[42] suggest a clear separation between malignant and non-malignant cells (Figure 3A). The cells from the two lymphoma cases clustered together (cluster M1 and M2) although representing different lymphoma subentities (Figure 3A). The integrated lymphoma cells displayed moderate expression of *CCR7* and *LEF1* reminiscent of naïve-like peripheral T cells[43], but did otherwise not exhibit a clear shared transcriptomic profile relating to a distinct functional canonical T cell subset (*Online Supplementary Figure 3 and Online*

Supplementary Figure 4). Profiling for T_{FH} markers, revealed *CD4* expression in the lymphoma samples (*Online Supplementary Figure 3*) and high levels of *ICOS* and *IL21* in the AITL case (*Online Supplementary Figure 5*). Notably, downregulation of *CCR7* as well as *LEF1* activity are associated with the initiation T_{FH} differentiation programs.[44,45] In line with the phenotype of circulating T_{FH} cells[44], we did not detect *BCL6* expression in the majority of cells (*Online Supplementary Figure 3*). Furthermore, lymphoma cells showed expression of T cell lymphoma-associated genes like *GATA3* and *TOX* and were characterized by high expression of *EPHB1*, *CYP46A1* and *TLR2* (*Online Supplementary Figure 3 and Online Supplementary Figure 4*). The receptor tyrosine kinase EPHB1 is linked to proliferation and metastasis in solid cancers[46], CYP46A1 acts in cholesterol biosynthesis linked to T cell lymphomas[47] and TLR2 is linked with T cell activation and has been demonstrated to lower the threshold required for TCR stimulation in CD8 T cells[48,49]. Next, we analyzed the distribution of TCR beta and alpha rearrangements at single-cell resolution in both patients separately (Figure 3B, C). Consistently with the bulk TCR sequencing analysis, the tumor cells of patient 055 showed monoclonality for a TRBV5-1 rearrangement, but also the alpha chain rearrangement was monoclonal (TRAV13-1 rearrangement). In line with this, the transcriptional profile was rather homogeneous in this case. Module expression of genes regulated by MYC, signal transduction by p53, TNF signaling and NFkB signaling was uniformly high in monoclonal T cells (Figure 3B). In patient 056, single-cell sequencing showed several distinct subclones with different configurations of the beta and alpha chain rearrangement. Two dominant beta and alpha TCR rearrangements were combined either with each other or with other combination partners and some of the cells showed more than one rearrangement per chain in their transcriptome suggesting expression of different TCR chimera in a single cell. Cells with a combination of the most dominant T cell receptor beta (TRBV3-1) and alpha (TRAV29/DV5) rearrangements showed transcriptomes that were more driven towards MYC and TGF

signaling (Figure 3C) as well as MAP kinase activity, histone modification and cell cycle activity (not shown). In contrast, cells with more aberrant TCR configurations with either more than one expressed rearrangement per locus or different rearrangements at the other locus were more driven towards JAK/STAT signaling and showed more overlap with non-malignant T cells (Figure 3C). This suggested that the transcriptomes expressed in this case were dictated by the respective TCR configuration (Figure 3C).

Together, this data demonstrates the broad spectrum of genetic and transcriptomic complexity in T cell lymphomas with the TCR configuration dictating downstream cellular programs in these diseases.

Variant allele frequencies of lymphoma driver mutations and TCR clonality demonstrates the sequence of transforming events

Next, we wished to assess the relationship between TCR clonality and lymphoma driver mutations. All cases with complete TCR sequencing and TRBV20-1 staining data were subjected to genomic profiling using a gene panel encompassing the most frequent T cell lymphoma driver alterations (*Online Supplementary Table 2*). This analysis revealed a total of 43 genomic alterations in 13 of 17 cases (Figure 4). Consistent with the literature, *TET2* mutations were present in 9 of 17 cases, *DNMT3A* in 2 of 17 cases.[50-53] Although all lymphomas were classified by an experienced reference pathologist, the frequent co-occurrence of *IDH2* and *RHOA* mutations in *TET2*-mutated in AITLs[54,55] was not reflected in our relatively small cohort. A comparison of variant allele frequencies (VAF) within the same patient revealed distinct patterns: certain genetic alterations were classified as founder lesions, likely present in every lymphoma cell, while others were classified as subclonal, indicating their presence in only a subset of cells. Notably, we observed that the clonal space defined by individual (sub)clonal driver mutations generally surpassed the size of the clonal space defined by specific subclonal TCR rearrangements (Figure 4). This

finding suggests that a single driver mutation serves as the foundation for the subsequent development of diverse subclones with heterogeneous TCR rearrangements in the majority of T cell lymphoma patients.

Clonal tiding

Finally, we explored clonal tiding of T cell lymphomas over the course of treatment. The analysis of TCR repertoire overlap between lymphoma tissue from the same patients at different time points suggested substantial clonal tiding with only limited clonal overlap at disease progressions. This is shown in exemplary patient 010 with four available samples at different time points (Figure 5A). While some clones were shared between the time points (marked in red), a substantial number of clones did not reappear in consecutive samples. Lymphoma tissue from different patients did not show any clonal overlap as shown in the control panel.

To investigate clonal dynamics on selective treatment pressure in more detail, we employed a case of AITL (patient 003) with multiple driver mutations that could be used as clonal barcodes. In this patient, three lymphoma samples were collected at three consecutive time points of disease progression. We hypothesized that the cellular co-occurrence of one or more driver lesions with a clonotypic TCR rearrangement would be reflected in synchronous expansion or contraction patterns over the disease course. Of note, while a cell may have multiple distinct driver mutations, it will only have one productive TCR rearrangement. To test for these patterns, we first plotted the dynamics of the 17 driver mutations that were found in this patient. As shown in Figure 5B, these mutations can be grouped into four dynamic patterns that either constantly contracted, expanded or showed mixed dynamics during progression. Next, we calculated the dynamics of the 547 unique TCR clonotypes that were found within the patient's lymphoma tissue at one of the sampled time points. For this, we used the normalized clonotype

frequencies over the time course and generated an Euclidean distant matrix. Using hierarchical clustering, we identified four distinct patterns of clonotype dynamics. We generated a PCA based on the normalized clonotype trajectories, color-coded the four different patterns and plotted their mean trajectories (Figure 5C). Surprisingly, the four trajectories matched exactly the four driver mutation trajectories. This implied that driver mutations and TCR clonotypes belonging to the same trajectory were very likely present in the same cell. While cluster 1 was defined by only one driver mutation, but 443 TCR clonotypes, cluster 2 showed four driver mutations along with 101 TCR rearrangements. Cluster 4 showed two driver mutations and two TCR rearrangements. The driver mutations must have been generated at a maturation stage prior to antigen receptor rearrangement in all of these three clusters given the number of TCR rearrangements associated with these. Finally, we assembled the information to illustrate the clonal landscape and its tiding from the first to the third relapse of patient 003 (Figure 5D). Together, this analysis showed that the dominant clone at diagnosis was replaced by alternative clones in the course of treatment.

Discussion

In the past decades, cancer research and especially massive genomic sequencing studies have contradicted the former paradigm of a linear evolution of malignancies. It has become clearer that the clonal evolution of solid tumors is driven by the development of different subclones emerging from immature cells leading to a complex and heterogeneous clonal landscape with its inherent potential for resistance. Hematological malignancies are traditionally conceived as less complex and an important number of these diseases are believed to derive from a mature cell of origin.

In the work presented, we challenged this view for a broad variety of T cell lymphoma entities. Almost half of our studied cases showed oligoclonality for the lymphoma TCR

rearrangements thereby confirming that the cell of origin of these “mature” neoplasms is in fact an immature precursor lymphocyte. This is in line with recent findings that suggest acquired driver mutations in hematopoietic progenitor cells as origin of malignant clones in Sézary syndrome.[56]

Moreover, the remarkable overrepresentation of TRBV20-1 rearrangements across all lymphoma subtypes suggested that this receptor configuration acts as a fundamentally relevant tumor driver in the development of these diseases.

Furthermore, this work provides insights in the evolution and shaping of the clonal lymphoma architecture under selective pressure of treatment by serial profiling of one lymphoma patient in the course of disease. In this exemplary case, the initially dominant clone was replaced by alternative clones under treatment pressure that could be demonstrated at the time point of first disease relapse. In the past years it has been frequently shown that specific treatments do not equally suppress all existing tumor subclones but may select for more aggressive, treatment-resistant clones.[57,58] The high clonal complexity of neoplastic diseases that already exist at the time point of diagnosis may provide the cause for this observation. Therefore, in this clonally complex diseases, profiling and therapeutic targeting of all coexisting disease subclones may be particularly important in the first-line setting while single-agent therapy may foster resistance. On the other hand, our concept of resistance as a permanent feature ascribed to a specific lymphoma and a specific drug may be revisited in light of our data. The replacement of the dominant clone by others in the course of treatment may open up the possibility of re-treatment with a regimen on which the patient has previously progressed. The establishment of clonal monitoring techniques that permit real-time clonality snapshots may, however, be a prerequisite for such personalized endeavors of guiding treatment.

Our work on lymphoma clonality may also be of relevance to guide the design of novel treatment approaches such as engineered cell products or bispecific antibodies. The vision

of using chimeric antigen receptor T cells for precision targeting of T cell lymphomas has failed so far on the lack of targets that are reliably expressed on the malignant T cell, but not on healthy T cells.[59,60] Recent studies demonstrated successful targeting of single TCR variable beta chains either with bispecific antibodies[61] or CAR T-cells[37] while leaving the postulated non-malignant T-cell compartment intact. However, our TCR clonality data calls for caution to use a single TCR rearrangement as reliable target due to the observed widespread oligoclonality and potential for regrowth from a more immature precursor cell with alternative TCR rearrangements.

Beyond its therapeutic implications, our research holds the potential to reshape the interpretation of studies conducted by others. In recent years, numerous single-cell sequencing studies focusing on T cell lymphomas have been published. However, only a minority of these studies sequenced unequivocal lymphoma cells characterized by an aberrant immunophenotype.[62] In the majority of manuscripts, classification was predominantly reliant on the identification of the most dominant TCR rearrangement, often leading to the categorization of cells with a divergent TCR rearrangement as non-malignant bystander cells as seen in Zhu et al[63] and Liu et al[64]. In light of the findings presented in our work, this prevailing paradigm must be questioned, urging a reassessment of the obtained results. This includes determination of matched TRA chains as well as TRG/D rearrangements, which were not covered in our analyses. Inclusion of these data may help to pinpoint the differentiation stage of the transformed precursor cell which can help to separate non-malignant bystander clonotypes and may have clinical relevance regarding phenotype plasticity.[14,65]

Taken together, our data confirm the high degree of clonal heterogeneity in T cell lymphomas with significant clonal tiding under selective therapeutic pressure. This data may foster our understanding of the complex nature of the clonal landscape and resistance in this group of diseases.

References

1. Alaggio R, Amador C, Anagnostopoulos I, et al. The 5th edition of the World Health Organization Classification of Haematolymphoid Tumours: Lymphoid Neoplasms. Leukemia. 2022;36(7):1720-1748.
2. Campo E, Jaffe ES, Cook JR, et al. The International Consensus Classification of Mature Lymphoid Neoplasms: a report from the Clinical Advisory Committee. Blood. 2022;140(11):1229-1253.
3. Fiore D, Cappelli LV, Broccoli A, Zinzani PL, Chan WC, Inghirami G. Peripheral T cell lymphomas: from the bench to the clinic. Nat Rev Cancer. 2020;20(6):323-342.
4. Dummer R, Vermeer MH, Scarisbrick JJ, et al. Cutaneous T cell lymphoma. Nat Rev Dis Primers. 2021;7(1):61.
5. Hague C, Farquharson N, Menasce L, Parry E, Cowan R. Cutaneous T-cell lymphoma: diagnosing subtypes and the challenges. Br J Hosp Med (Lond). 2022;83(4):1-7.
6. Park HS, McIntosh L, Braschi-Amirfarzan M, Shinagare AB, Krajewski KM. T-Cell Non-Hodgkin Lymphomas: Spectrum of Disease and the Role of Imaging in the Management of Common Subtypes. Korean J Radiol. 2017;18(1):71-83.
7. Broccoli A, Zinzani PL. Peripheral T-cell lymphoma, not otherwise specified. Blood. 2017;129(9):1103-1112.
8. Marks DI, Rowntree C. Management of adults with T-cell lymphoblastic leukemia. Blood. 2017;129(9):1134-1142.
9. Izykowska K, Rassek K, Korsak D, Przybylski GK. Novel targeted therapies of T cell lymphomas. J Hematol Oncol. 2020;13(1):176.
10. Bellei M, Foss FM, Shustov AR, et al. The outcome of peripheral T-cell lymphoma patients failing first-line therapy: a report from the prospective, International T-Cell Project. Haematologica. 2018;103(7):1191-1197.
11. Chihara D, Fanale MA, Miranda RN, et al. The survival outcome of patients with relapsed/refractory peripheral T-cell lymphoma-not otherwise specified and angioimmunoblastic T-cell lymphoma. Br J Haematol. 2017;176(5):750-758.
12. Lansigan F, Horwitz SM, Pinter-Brown LC, et al. Outcomes for Relapsed and Refractory Peripheral T-Cell Lymphoma Patients after Front-Line Therapy from the COMPLETE Registry. Acta Haematol. 2020;143(1):40-50.
13. Stuver R, Moskowitz AJ. Therapeutic Advances in Relapsed and Refractory Peripheral T-Cell Lymphoma. Cancers (Basel). 2023;15(3):589.
14. Iyer A, Hennessey D, Gniadecki R. Clonotype pattern in T-cell lymphomas map the cell of origin to immature lymphoid precursors. Blood Adv. 2022;6(7):2334-2345.
15. Marks JA, Switchenko JM, Martini DJ, et al. T-Cell Receptor Gene Rearrangement Clonality, Flow Cytometry Status, and Associated Outcomes in Early-Stage Cutaneous T-Cell Lymphoma. JAMA Dermatol. 2021;157(8):954-962.
16. Vose J, Armitage J, Weisenburger D, International TCLP. International peripheral T-cell and natural killer/T-cell lymphoma study: pathology findings and clinical outcomes. J Clin Oncol. 2008;26(25):4124-4130.
17. Zain JM, Hanona P. Aggressive T-cell lymphomas: 2021 Updates on diagnosis, risk stratification and management. Am J Hematol. 2021;96(8):1027-1046.
18. Krangel MS. Mechanics of T cell receptor gene rearrangement. Curr Opin Immunol. 2009;21(2):133-139.
19. Attygalle AD, Kyriakou C, Dupuis J, et al. Histologic evolution of angioimmunoblastic T-cell lymphoma in consecutive biopsies: clinical correlation and insights into natural history and disease progression. Am J Surg Pathol. 2007;31(7):1077-1088.

20. Chiba S, Sakata-Yanagimoto M. Advances in understanding of angioimmunoblastic T-cell lymphoma. Leukemia. 2020;34(10):2592-2606.
21. Grogg KL, Attygalle AD, Macon WR, Remstein ED, Kurtin PJ, Dogan A. Angioimmunoblastic T-cell lymphoma: a neoplasm of germinal-center T-helper cells? Blood. 2005;106(4):1501-1502.
22. Yao WQ, Wu F, Zhang W, et al. Angioimmunoblastic T-cell lymphoma contains multiple clonal T-cell populations derived from a common TET2 mutant progenitor cell. J Pathol. 2020;250(3):346-357.
23. Couronne L, Bastard C, Bernard OA. TET2 and DNMT3A mutations in human T-cell lymphoma. N Engl J Med. 2012;366(1):95-96.
24. Quivoron C, Couronne L, Della Valle V, et al. TET2 inactivation results in pleiotropic hematopoietic abnormalities in mouse and is a recurrent event during human lymphomagenesis. Cancer Cell. 2011;20(1):25-38.
25. Zhang X, Su J, Jeong M, et al. DNMT3A and TET2 compete and cooperate to repress lineage-specific transcription factors in hematopoietic stem cells. Nat Genet. 2016;48(9):1014-1023.
26. Cheng S, Zhang W, Inghirami G, Tam W. Mutation analysis links angioimmunoblastic T-cell lymphoma to clonal hematopoiesis and smoking. Elife. 2021;10:e66395.
27. Sandell RF, Boddicker RL, Feldman AL. Genetic Landscape and Classification of Peripheral T Cell Lymphomas. Curr Oncol Rep. 2017;19(4):28.
28. Vega F, Amador C, Chadburn A, et al. Genetic profiling and biomarkers in peripheral T-cell lymphomas: current role in the diagnostic work-up. Mod Pathol. 2022;35(3):306-318.
29. Schultheiss C, Simnica D, Willscher E, et al. Next-Generation Immunosequencing Reveals Pathological T-Cell Architecture in Autoimmune Hepatitis. Hepatology. 2021;73(4):1436-1448.
30. Simnica D, Akyuz N, Schliffke S, et al. T cell receptor next-generation sequencing reveals cancer-associated repertoire metrics and reconstitution after chemotherapy in patients with hematological and solid tumors. Oncoimmunology. 2019;8(11):e1644110.
31. Simnica D, Schliffke S, Schultheiss C, et al. High-Throughput Immunogenetics Reveals a Lack of Physiological T Cell Clusters in Patients With Autoimmune Cytopenias. Front Immunol. 2019;10:1897.
32. Bolotin DA, Poslavsky S, Mitrophanov I, et al. MiXCR: software for comprehensive adaptive immunity profiling. Nat Methods. 2015;12(5):380-381.
33. Schultheiss C, Paschold L, Simnica D, et al. Next-Generation Sequencing of T and B Cell Receptor Repertoires from COVID-19 Patients Showed Signatures Associated with Severity of Disease. Immunity. 2020;53(2):442-455.
34. Schumann FL, Gross E, Bauer M, et al. Divergent Effects of EZH1 and EZH2 Protein Expression on the Prognosis of Patients with T-Cell Lymphomas. Biomedicines. 2021;9(12):1842.
35. Meyer-Olson D, Simons BC, Conrad JA, et al. Clonal expansion and TCR-independent differentiation shape the HIV-specific CD8+ effector-memory T-cell repertoire in vivo. Blood. 2010;116(3):396-405.
36. Ciupe SM, Devlin BH, Markert ML, Kepler TB. Quantification of total T-cell receptor diversity by flow cytometry and spectratyping. BMC Immunol. 2013;14:35.
37. Ren J, Liao X, Lewis JM, et al. Generation and optimization of off-the-shelf immunotherapeutics targeting TCR-Vbeta2+ T cell malignancy. Nat Commun. 2024;15(1):519.
38. Bauer M, Vaxevanis C, Bethmann D, et al. Multiplex immunohistochemistry as a novel tool for the topographic assessment of the bone marrow stem cell niche. Methods Enzymol. 2020;635:67-79.
39. Schultheiss C, Paschold L, Willscher E, et al. Maturation trajectories and transcriptional landscape of plasmablasts and autoreactive B cells in COVID-19. iScience. 2021;24(11):103325.
40. Wang P, Jin X, Zhou W, et al. Comprehensive analysis of TCR repertoire in COVID-19 using single cell sequencing. Genomics. 2021;113(2):456-462.
41. Herrera A, Cheng A, Mimitou EP, et al. Multimodal single-cell analysis of cutaneous T-cell lymphoma reveals distinct subclonal tissue-dependent signatures. Blood. 2021;138(16):1456-1464.

42. 10x Genomics. Integrated GEX and VDJ analysis of Connect generated library from human PBMCs by Cell Ranger 6.0.1; 2021. https://www.10xgenomics.com/datasets/integrated-gex-and-vdj-analysis-of-connect-generated-library-from-human-pbm-cs-2-standard-6-0-1 Accessed on January 2024
43. Willinger T, Freeman T, Herbert M, Hasegawa H, McMichael AJ, Callan MF. Human naive CD8 T cells down-regulate expression of the WNT pathway transcription factors lymphoid enhancer binding factor 1 and transcription factor 7 (T cell factor-1) following antigen encounter in vitro and in vivo. J Immunol. 2006;176(3):1439-1446.
44. Vinuesa CG, Linterman MA, Yu D, MacLennan IC. Follicular Helper T Cells. Annu Rev Immunol. 2016;34:335-368.
45. Choi YS, Gullicksrud JA, Xing S, et al. LEF-1 and TCF-1 orchestrate T(FH) differentiation by regulating differentiation circuits upstream of the transcriptional repressor Bcl6. Nat Immunol. 2015;16(9):980-990.
46. Pasquale EB. Eph receptors and ephrins in cancer: bidirectional signalling and beyond. Nat Rev Cancer. 2010;10(3):165-180.
47. Mehta A, Ratre YK, Soni VK, et al. Orchestral role of lipid metabolic reprogramming in T-cell malignancy. Front Oncol. 2023;13:1122789.
48. Salerno F, Freen-van Heeren JJ, Guislain A, Nicolet BP, Wolkers MC. Costimulation through TLR2 Drives Polyfunctional CD8(+) T Cell Responses. J Immunol. 2019;202(3):714-723.
49. Morrison C, Baer MR, Zandberg DP, Kimball A, Davila E. Effects of Toll-like receptor signals in T-cell neoplasms. Future Oncol. 2011;7(2):309-320.
50. Heavican TB, Bouska A, Yu J, et al. Genetic drivers of oncogenic pathways in molecular subgroups of peripheral T-cell lymphoma. Blood. 2019;133(15):1664-1676.
51. Odejide O, Weigert O, Lane AA, et al. A targeted mutational landscape of angioimmunoblastic T-cell lymphoma. Blood. 2014;123(9):1293-1296.
52. Watatani Y, Sato Y, Miyoshi H, et al. Molecular heterogeneity in peripheral T-cell lymphoma, not otherwise specified revealed by comprehensive genetic profiling. Leukemia. 2019;33(12):2867-2883.
53. Rodriguez M, Alonso-Alonso R, Tomas-Roca L, et al. Peripheral T-cell lymphoma: molecular profiling recognizes subclasses and identifies prognostic markers. Blood Adv. 2021;5(24):5588-5598.
54. Leca J, Lemonnier F, Meydan C, et al. IDH2 and TET2 mutations synergize to modulate T Follicular Helper cell functional interaction with the AITL microenvironment. Cancer Cell. 2023;41(2):323-339.
55. Sakata-Yanagimoto M, Enami T, Yoshida K, et al. Somatic RHOA mutation in angioimmunoblastic T cell lymphoma. Nat Genet. 2014;46(2):171-175.
56. Harro CM, Sprenger KB, Chaurio RA, et al. Sezary syndrome originates from heavily mutated hematopoietic progenitors. Blood Adv. 2023;7(18):5586-5602.
57. Keats JJ, Chesi M, Egan JB, et al. Clonal competition with alternating dominance in multiple myeloma. Blood. 2012;120(5):1067-1076.
58. Clemente MJ, Wlodarski MW, Makishima H, et al. Clonal drift demonstrates unexpected dynamics of the T-cell repertoire in T-large granular lymphocyte leukemia. Blood. 2011;118(16):4384-4393.
59. To V, Evtimov VJ, Jenkin G, Pupovac A, Trounson AO, Boyd RL. CAR-T cell development for Cutaneous T cell Lymphoma: current limitations and potential treatment strategies. Front Immunol. 2022;13:968395.
60. Oh BLZ, Vinanica N, Wong DMH, Campana D. Chimeric antigen receptor T-cell therapy for T-cell acute lymphoblastic leukemia. Haematologica. 2024;109(6):1677-1688.
61. Paul S, Pearlman AH, Douglass J, et al. TCR beta chain-directed bispecific antibodies for the treatment of T cell cancers. Sci Transl Med. 2021;13(584):eabd3595.
62. Suma S, Suehara Y, Fujisawa M, et al. Tumor heterogeneity and immune-evasive T follicular cell lymphoma phenotypes at single-cell resolution. Leukemia. 2024;38(2):340-350.

63. Zhu Q, Yang Y, Deng X, et al. High CD8(+)tumor-infiltrating lymphocytes indicate severe exhaustion and poor prognosis in angioimmunoblastic T-cell lymphoma. Front Immunol. 2023;14:1228004.
64. Liu X, Jin S, Hu S, et al. Single-cell transcriptomics links malignant T cells to the tumor immune landscape in cutaneous T cell lymphoma. Nat Commun. 2022;13(1):1158.
65. Iyer A, Hennessey D, O'Keefe S, et al. Clonotypic heterogeneity in cutaneous T-cell lymphoma (mycosis fungoides) revealed by comprehensive whole-exome sequencing. Blood Adv. 2019;3(7):1175-1184.

Tables

Table 1. Characteristics of T cell lymphoma cohort

	TCR-NGS* cohort	TMA** cohort
Nb of patients	21	50
Nb of samples	27	68
Sex		
Female	5/21	16/50
Male	16/21	34/50
Median age (range)	67y (36-92)	66y (36-92)
T-NHL subtype		
Angioimmunoblastic T cell lymphoma (AITL)	12/21	15/50
Peripheral T cell lymphoma, not otherwise specified (PTCL, NOS)	6/21	14/50
T cell prolymphocytic leukemia (T-PLL)	2/21	1/50
T cell large granular lymphocytic leukemia (T-LGLL)	1/21	2/50
Anaplastic large-cell lymphoma (ALCL)	0/21	7/50
PTCL with T follicular helper phenotype (PTCL-TFH)	0/21	3/50
Sézary syndrome (SS)	0/21	2/50
Monomorphic epitheliotropic intestinal T cell lymphoma (MEITL)	0/21	1/50
Mycosis fungoides (MF)	0/21	1/50
Extranodal NK/T cell lymphoma, nasal type (ENKL)	0/21	1/50
Post-transplant lymphoproliferative disorder (PTLD)	0/21	1/50
Enteropathy-associated T cell lymphoma (EATL)	0/21	1/50
Subcutaneous panniculitis-like T cell lymphoma (SPTCL)	0/21	1/50

*TCR-NGS = T cell receptor next generation sequencing **TMA = Tissue microarray

Figure Legends

Figure 1. Immunosequencing of T cell receptor (TCR) repertoires of T cell lymphoma tissue. (A) TCR repertoire metrics of healthy blood (n=121) and lymphoma tissue (n=19). For patients with multiple samples, the earliest time point was used. Statistics: ANOVA (B) Frequency of unique V(D)J rearrangements in selected individual repertoires. Each dot represents a unique rearranged complementarity-determining region 3 (CDR3) amino acid sequence where radius reflects clone size in repertoire. (C) Proportions of mono- and oligoclonal cases within the analyzed T cell lymphoma cohort (n=19) and number of cumulative clones per repertoire matching tumor cell fraction. (D) Principal component analysis (PCA) of V gene usage in lymphoma tissue samples (red, n=19) and healthy blood samples (blue, n=121). Bars show the top 10 contributing V genes responsible for group differences at principal component 2. Dashed line indicates threshold. Statistics: Manova over PCA with pillai trace. (E) Frequencies of TRBV20-1 gene usage in the T cell lymphoma samples (n=19). TRBV20-1 frequencies in the blood of patients with acute COVID-19 infection (n=19) or healthy individuals (n=121) as controls. (F) TCR repertoire metrics for lymphoma samples at initial diagnosis (ID) and after progression. Statistics: ANOVA

Figure 2. Tissue microarray staining of T cell lymphomas for TRBV20-1 expression. (A) DAPI staining was performed to localize section borders. TRBV20-1 gene signals were classified as homogeneously positive (a), patchy distributed (b) or negative (c). 123x magnification of indicated examples on the right. Scale bar represents 200 µm. (B) Left panel: TRBV20-1 frequency (NGS) and grouped total cell fluorescence for TRBV20-1. Right panel: Summary of detected TRBV20-1 staining pattern per lymphoma entity.

Figure 3. Single-cell ananlysis of sorted lymphoma cells from two patients. (A) t-distributed stochastic neighbor embedding (tSNE) plot of integrated single-cell RNA data set encompassing 985 lymphoma T cells from a patient with T prolymphocytic leukemia (T-PLL) (055), 479 lymphoma T cells from a patient with angioimmunoblastic T cell lymphoma (AITL) (056) and 4373 T cells from two healthy donors. Cells are colored by cluster or sample origin. M1: Malignant cluster one; M2: malignant cluster two; T4N: naïve $CD4^+$ T cells; T4: $CD4^+$ T cells; CM: central memory T cells; gdT: γδT cells; aT8: activated $CD8^+$ T cells; TC17-like: IL17 producing-like $CD8^+$ T cells; cT: cytotoxic T cells; Th1: Th1 T cells. (B) Uniform manifold approximation and projection (UMAP) plot of reclustered lymphoma cells from patient 055. Characterizing expression programs of the malignant cells shown as feature plot after scoring (Seurat *addmodulescore* function) of indicated GO gene sets. The clonotypic TRA and TRB rearrangements per cluster are shown in red in the lower UMAP. Proportions of these cells within each cluster (C1-6) are depicted in the stacked bar plot. (C) UMAP of lymphoma cells from patient 056 as presented in (B). T cells with at least one clonotypic TCR rearrangement are highlighted in color within the UMAP. Proportion of cells with at least one clonotypic rearrangement are depicted in the stacked bar plot per cluster (C1-5).

Figure 4. Overview matrix over T cell receptor (TCR) clonality of the respective dominant clone and variant allele frequency of each detected single mutation in all

evaluable samples. VAF = variant allele frequency, AITL = angioimmunoblastic T cell lymphoma, T-LGLL = T cell large granular lymphocytic leukemia, PTCL NOS = peripheral T cell lymphomas not otherwise specified

Figure 5. Clonal tiding of T cell lymphomas over the course of treatment. (A) Clonal overlap in lymphoma specimen from patient 010 sampled at different timepoints during the course of the disease. Shared identical TCR rearrangements are displayed in red. A control plot shows the lack of TCR overlap between lymphoma tissue of different patients. (B) Four different dynamic patterns (indicated as purple, green, yellow, red) of 17 driver mutations in a case of AITL (patient 003) over the course of treatment as determined using gene panel sequencing. (C) Clustering and Principal Component Analysis (PCA) of the 547 unique TCR clonotypes of AITL patient 003 present at all sampled time points in the lymphoma tissue. The dynamic trajectories of the clustered clonotypes are shown on the right. (D) Illustration of the assembled mutational and clonal information over three disease progressions. Circle size represents cumulative variant allele frequency (VAF) of mutations.

Figure 1

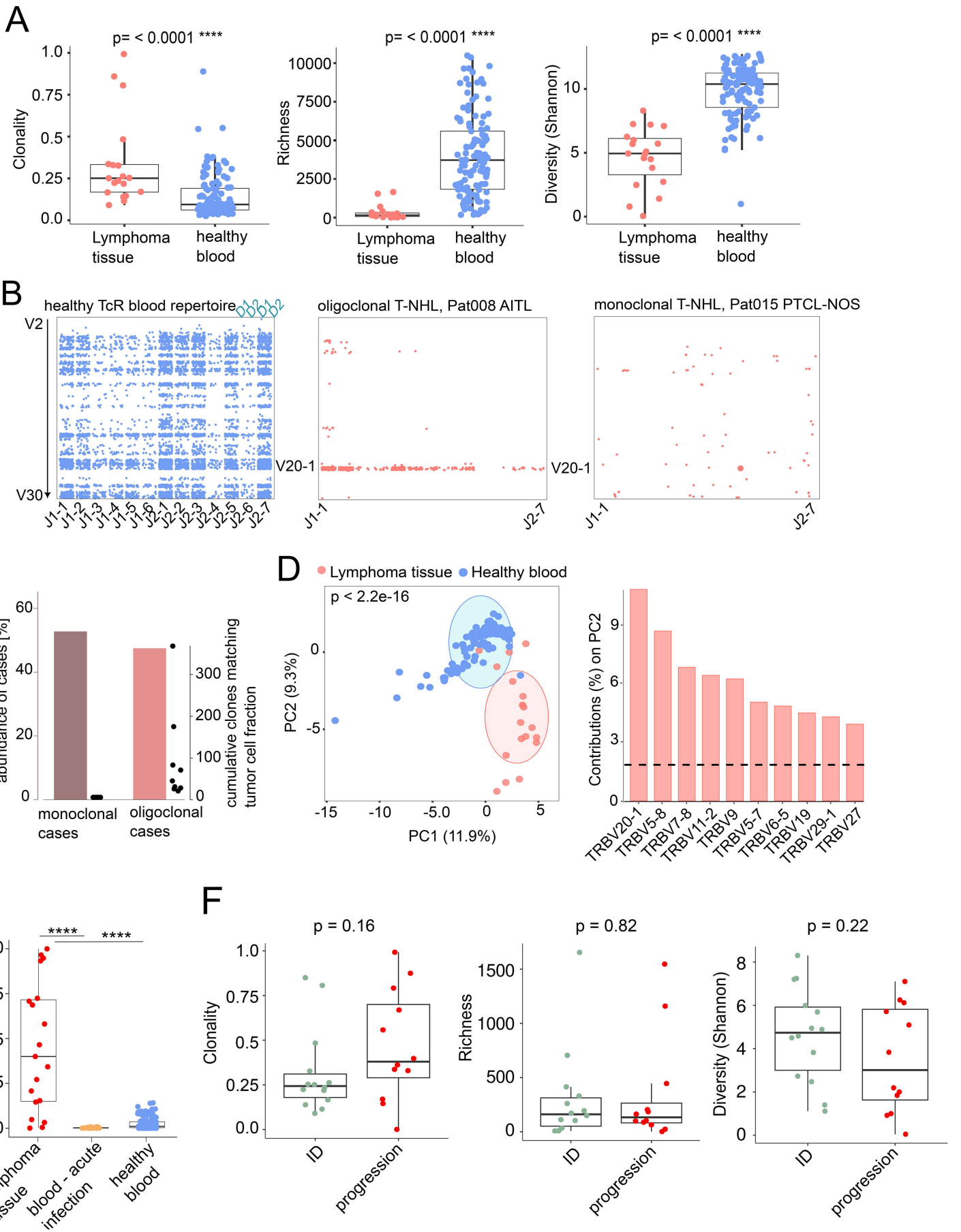
A
p= < 0.0001 ****
Clonality
Lymphoma tissue
healthy blood
p= < 0.0001 ****
Richness
Lymphoma tissue
healthy blood
p= < 0.0001 ****
Diversity (Shannon)
Lymphoma tissue
healthy blood
B
healthy TcR blood repertoire
V2
V30
oligoclonal T-NHL, Pat008 AITL
V20-1
J1-1
J2-7
monoclonal T-NHL, Pat015 PTCL-NOS
V20-1
J1-1
J2-7
C
abundance of cases [%]
cumulative clones matching tumor cell fraction
monoclonal cases
oligoclonal cases
D
Lymphoma tissue
Healthy blood
p < 2.2e-16
PC2 (9.3%)
PC1 (11.9%)
Contributions (%) on PC2
TRBV20-1
TRBV5-8
TRBV7-8
TRBV11-2
TRBV9
TRBV5-7
TRBV6-5
TRBV19
TRBV29-1
TRBV27
E
****
****
TRBV20-1 frequency
Lymphoma tissue
blood - acute infection
healthy blood
F
p = 0.16
Clonality
ID
progression
p = 0.82
Richness
ID
progression
p = 0.22
Diversity (Shannon)
ID
progression

Figure 2

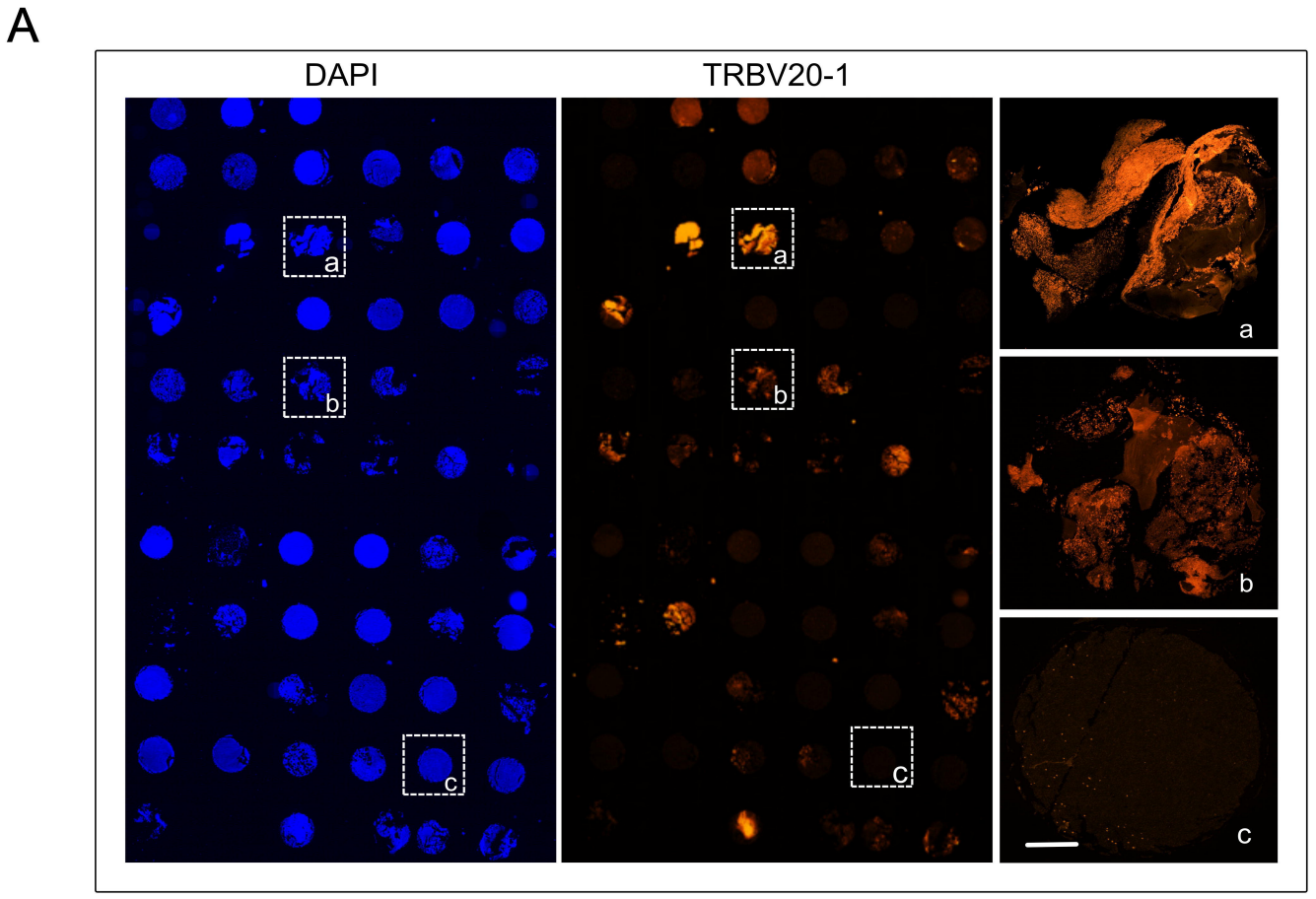
A
DAPI
TRBV20-1
a
b
c
a
b
c
a
b
c
B
p = 0.16
TRBV20-1 frequency
1.00
0.75
0.50
0.25
0
positive
partially positive/ negative
TRBV20-1 staining analysis of Tissue Microarray
Nb of samples
20
15
10
5
0
AITL
PTCL, NOS
ALCL
MEITL
T-LGLL
PTCL TFH
NKTCL
SS
T-PLL
EATL
SPTCL
MF
positive
partially positive /negative

Figure 3

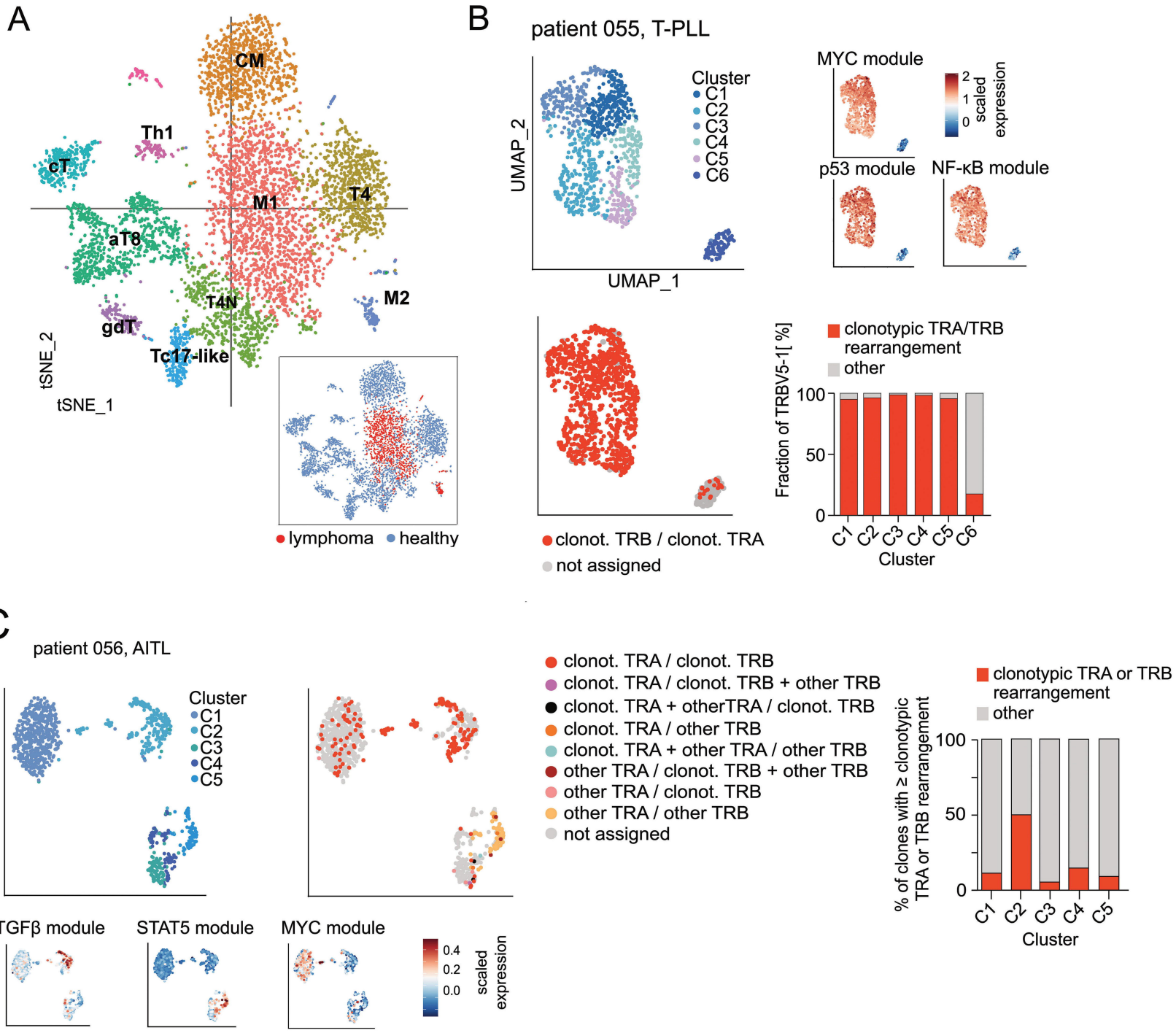
A
CM
Th1
cT
M1
T4
aT8
T4N
M2
gdT
Tc17-like
tSNE_2
tSNE_1
lymphoma
healthy
B
patient 055, T-PLL
Cluster
C1
C2
C3
C4
C5
C6
UMAP_2
UMAP_1
MYC module
p53 module
NF-κB module
scaled expression
clonot. TRB / clonot. TRA
not assigned
clonotypic TRA/TRB rearrangement
other
Fraction of TRBV5-1[%]
Cluster
C
patient 056, AITL
TGFβ module
STAT5 module
MYC module
clonot. TRA / clonot. TRB
clonot. TRA / clonot. TRB + other TRB
clonot. TRA + otherTRA / clonot. TRB
clonot. TRA / other TRB
clonot. TRA + other TRA / other TRB
other TRA / clonot. TRB + other TRB
other TRA / clonot. TRB
other TRA / other TRB
not assigned
clonotypic TRA or TRB rearrangement
other
% of clones with ≥ clonotypic TRA or TRB rearrangement
Cluster

Figure 4

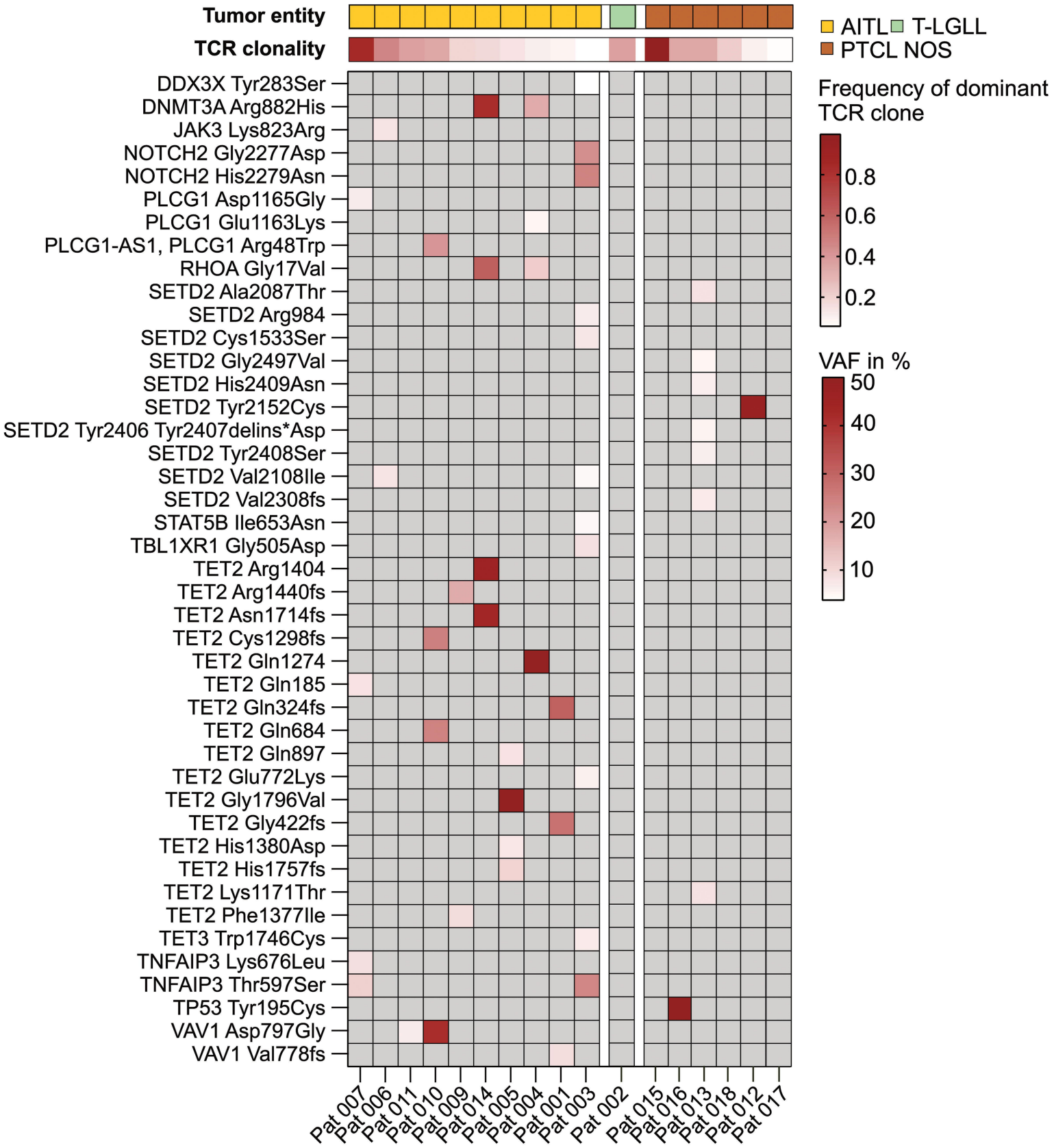
Tumor entity
TCR clonality
AITL
T-LGLL
PTCL NOS
Frequency of dominant TCR clone
0.8
0.6
0.4
0.2
VAF in %
50
40
30
20
10
DDX3X Tyr283Ser
DNMT3A Arg882His
JAK3 Lys823Arg
NOTCH2 Gly2277Asp
NOTCH2 His2279Asn
PLCG1 Asp1165Gly
PLCG1 Glu1163Lys
PLCG1-AS1, PLCG1 Arg48Trp
RHOA Gly17Val
SETD2 Ala2087Thr
SETD2 Arg984
SETD2 Cys1533Ser
SETD2 Gly2497Val
SETD2 His2409Asn
SETD2 Tyr2152Cys
SETD2 Tyr2406 Tyr2407delins*Asp
SETD2 Tyr2408Ser
SETD2 Val2108Ile
SETD2 Val2308fs
STAT5B Ile653Asn
TBL1XR1 Gly505Asp
TET2 Arg1404
TET2 Arg1440fs
TET2 Asn1714fs
TET2 Cys1298fs
TET2 Gln1274
TET2 Gln185
TET2 Gln324fs
TET2 Gln684
TET2 Gln897
TET2 Glu772Lys
TET2 Gly1796Val
TET2 Gly422fs
TET2 His1380Asp
TET2 His1757fs
TET2 Lys1171Thr
TET2 Phe1377Ile
TET3 Trp1746Cys
TNFAIP3 Lys676Leu
TNFAIP3 Thr597Ser
TP53 Tyr195Cys
VAV1 Asp797Gly
VAV1 Val778fs
Pat 007
Pat 006
Pat 011
Pat 010
Pat 009
Pat 014
Pat 005
Pat 004
Pat 001
Pat 003
Pat 002
Pat 015
Pat 016
Pat 013
Pat 018
Pat 012
Pat 017

Figure 5

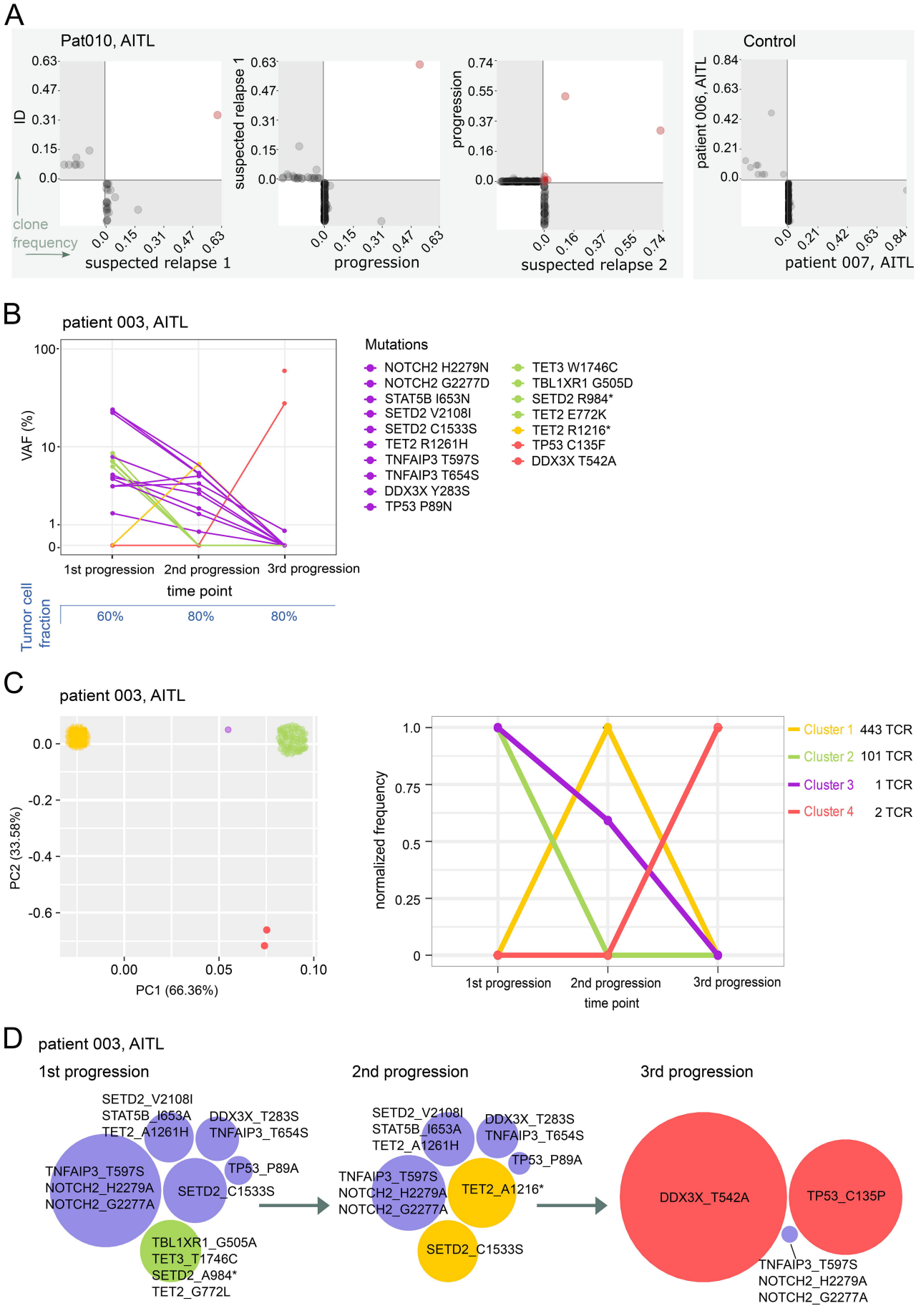
A
Pat010, AITL
ID
suspected relapse 1
progression
suspected relapse 2
clone frequency
Control
patient 006, AITL
patient 007, AITL
B
patient 003, AITL
VAF (%)
1st progression
2nd progression
3rd progression
time point
Tumor cell fraction
60%
80%
80%
Mutations
NOTCH2 H2279N
NOTCH2 G2277D
STAT5B I653N
SETD2 V2108I
SETD2 C1533S
TET2 R1261H
TNFAIP3 T597S
TNFAIP3 T654S
DDX3X Y283S
TP53 P89N
TET3 W1746C
TBL1XR1 G505D
SETD2 R984*
TET2 E772K
TET2 R1216*
TP53 C135F
DDX3X T542A
C
patient 003, AITL
PC2 (33.58%)
PC1 (66.36%)
normalized frequency
time point
Cluster 1 443 TCR
Cluster 2 101 TCR
Cluster 3 1 TCR
Cluster 4 2 TCR
D
patient 003, AITL
1st progression
SETD2_V2108I
STAT5B_I653A
TET2_A1261H
DDX3X_T283S
TNFAIP3_T654S
TNFAIP3_T597S
NOTCH2_H2279A
NOTCH2_G2277A
TP53_P89A
SETD2_C1533S
TBL1XR1_G505A
TET3_T1746C
SETD2_A984*
TET2_G772L
2nd progression
SETD2_V2108I
STAT5B_I653A
TET2_A1261H
DDX3X_T283S
TNFAIP3_T654S
TP53_P89A
TNFAIP3_T597S
NOTCH2_H2279A
NOTCH2_G2277A
TET2_A1216*
SETD2_C1533S
3rd progression
DDX3X_T542A
TP53_C135P
TNFAIP3_T597S
NOTCH2_H2279A
NOTCH2_G2277A

Supplementary Methods:

T cell receptor (TCR) immune repertoire sequencing and data analysis

The ReliaPrep™ FFPE gDNA Miniprep System (Promega, Madison, United States) was used for isolation of genomic DNA from FFPE tissue. The V(D)J rearranged TRBV loci were amplified in a multiplex PCR using the Phusion™ High-Fidelity DNA Polymerase (Thermo Fisher Scientific, Waltham, USA) and the BIOMED2-FR2/FR3 -TRB-B primer pools. The primers were purchased from Metabion International AG (Martinsried, Germany). PCR amplicons were purified using the Agencourt AMPure XP paramagnetic beads (Beckman Coulter) and subjected to a second PCR for the addition of 7-nucleotide single indices and Illumina adapter sequences. After bead-based purification, PCR amplicons were quantified using the Qubit system (Thermo Fisher) and pooled to a final concentration of six nM. Pools were quality controlled on an Agilent 2100 Bioanalyzer (Agilent Technologies, Böblingen, Germany). Sequencing and demultiplexing was performed on an Illumina MiSeq sequencer (Illumina, San Diego, USA) with a 601-cycle paired-end run and V3-chemistry. The MiXCR framework[1] v.3.0.12 was used for sequence alignment and clonotype assignment. Non-productive reads and clonotypes with less than two reads were discarded. Each unique nucleotide CDR3 sequence was considered a clone. For analysis of repertoire metrics, healthy immune repertoires were proportionally normalized to 30,000 productive reads. Clonality of TRB repertoires was calculated according to the formula 1- H'/log2(S) with H' being the Shannon diversity index and S the total number of TRB clonotypes (=richness) in an individual repertoire. Principal component analysis (PCA) of V Gene usage and their contributions were calculated using R package ade4. Data analysis and plotting was performed with Rstudio (version 2023.03.1+446). Monoclonality was assumed if the frequency of the most abundant clonotype in the repertoire matched the respective tumor cell fraction of the sample (+/-20%). Moreover, monoclonality was assumed if the frequency

of the first two clonotypes of the repertoire showed a frequency that matched the tumor cell fraction (+/-20%), but only if these two clonotypes had a similar frequency (+/-20%) to account for biallelic rearrangements. All other cases were classified as oligoclonal. Tumor cell fraction was determined by a reference pathologist.

Dynamics of TCR clones

Longitudinal dynamics of lymphoma subclones from patient 003 were calculated according to the approach by Minervina et al[2,3]. For this, a Euclidean distance matrix of the normalized frequencies of the top 1000 TCR clonotypes for each sampling time point was generated. Clusters were then identified using hierachical clustering and visualized over time using PCA. Mean trajectories for all four patterns were shown at normalized frequencies.

Tissue microarray staining for TRBV20-1 usage

Available FFPE tissue from our TCR NGS cohort as well as additional T cell lymphoma samples were analyzed using a tissue microarray as reported by Schümann et al[4]. Antigen retrieval was performed using a TRIS-EDTA Buffer pH 9.0 antigen retrieval solution (ZUC029-500, Zytomed, Germany) followed by a blocking step (ZUC007-100, Zytomed, Germany). The TCR Vβ2-PE antibody (diluted 1:100, IM2213, Beckmann Coulter, CA, USA) was incubated at room temperature for 60 minutes and a counterstaining with DAPI (Akoya Biosciences, MA, USA) was performed as described in Bauer et al[5]. After a washing step, all slides were mounted with Vectashield Antifade Mounting Medium (H-1000-10, Vector Laboratories, CA; USA) and visualized with a PhenoImager HT (Akoya Biosciences, MA, USA). Tissue microarray (TMA) spot intensity was determined using ImageJ (National Institutes of Health) according to the online protocol provided by the Keith R. Porter Imaging Facility.[6]

Gene panel profiling

Profiling of hotspots mutations associated with T cell lymphomas was performed using a targeted DNA Custom Panels from Qiagen (Hilden, Germany). Genes with recurrent mutations in T cell lymphoma were selected from cbioportal (Supplementary Table S2). Sequencing libraries were constructed using Qiaseq Targeted DNA Custom Panels (Qiagen, Hilden, Germany). The Qubit high-sensitivity double-strand DNA assay kit (Thermo Fisher) was used for quantification of libraries and the Agilent 2100 Bioanalyzer (Agilent) for final quality control. Libraries were sequenced on a Illumina NextSeq 500 platform with 2 x 150 cycles at an average coverage of 52,700 reads per target region. Variant calling of unique molecular identifier (UMI) was performed using CLC Workbench (Quiagen). Mutations were considered as positive if they were found with a variant allele frequency (VAF) exceeding 10% at a read depth of more than 70 reads. To filter for disease relevant mutations, common single nucleotide polymorphisms (SNPs) stated by dbSNP were discarded as well as synonymous variants.

Cell sorting and single-cell transcriptomic profiling

Sorting of lymphoma cells was performed based on their aberrant CD4+/CD8+ immunophenotype (T-PLL case) or on aberrant CD3 surface expression (AITL case) from cryopreserved peripheral blood mononuclear cells (PBMCs) of these two T cell lymphoma patients. For that, the anti-CD3-APC-H7 (clone SK7, BD Biosciences), anti-CD4-PacificBlue (clone RPA-T4, Biolegend) and the anti-CD8-FITC (clone SK1, BD Biosciences) antibodies were used on a BD FACSAriaIII cell sorter with a 100 µm nozzle. Cells were processed on a 10X Chromium Controller (10X Genomics, Pleasanton, CA, USA) within 1h after collection. Single-cell libraries were generated using the Next GEM Single Cell 5' Kit v2 and Chromium Single Cell Human TCR Amplification kits according to the manufacturer instructions to

detect coupled TCR beta and alpha chains. For the integrated dataset we used two healthy samples provided in Herrera et al[7] (sample HC1) and one 10X resource dataset.[8] The two lymphoma samples and the two healthy samples were merged together using package Seurat (v 5.0.0).[9] Cells with high mitochondrial content (>10%) and more than 2500 RNA features were excluded. Normalization and detection of the top 2000 variable features was done individually for each dataset. To merge data sets, integration anchors were calculated using function *FindIntegrationAnchors* and datasets were integrated with *IntegrateData* to one object. After scaling, PCA and t-distributed stochastic neighbor embedding (tSNE) calculation were performed on 15 dimensions. T cell clusters were assigned according to subset markers found with function *FindAllMarkers* and selected T cell population marker genes. Module scores for feature expression programs were calculated with function *AddModuleScore*. The modules contained following genes: the MYC module contains targets of MYC (CCT3, DUT, RPL34, RPS5, RPL22, RPLP0, RPS6, RPL6, EEF1B2, FBL, SNRPD2, RACK1, RPS3, RPL14, RPS2, RPL18, RPS10, PPIA, EIF3D); the p53 module comprises genes which regulate signal transduction by p53 positively (RPS15, RPS7, UBB, RPL23, RPS20, RPL37); the NF-kB module contains genes, which are expressed when NFkB is activated (UBB,UBC,RACK1,RPS27A,UBA52); TGFb module encloses genes of the TGFb pathway (APP, MAP2K4, MAP2K1, CREBBP, SMAD4, SMURF2, SMURF1, ITGA2, LIMK2, NEDD4L, NEDD9, NUP153, MAPK14, RUNX2, PIAS2, PIAS1, TGFBR3, SKI, MAPK8, RBL1, BTRC, MAP2K6); the STAT5 module contains genes involved in IL2/STAT5 signaling (PHTF2, ABCB1, AHNAK, PTGER2, CTSZ, FURIN, CST7, NDRG1, SOCS2, NFKBIZ, PIM1, LRIG1, CTLA4, SNX9, MAP3K8, ITGAV, TNFRSF4, GABARAPL1, IL4R, GADD45B, CISH, NCOA3, IL10RA, TNFRSF18, FLT3LG, RHOH, TNFRSF1B, IGF2R, HOPX, SERPINB6, IL2RA, BHLHE40, BCL2, LTB, IL18R1).

Fastq files from V(D)J libraries were analysed with cellranger vdj pipeline, and the filtered results were integrated with gene expression data with package scRepertoire (v 1.4.0).

1. Bolotin DA, Poslavsky S, Mitrophanov I, et al. MiXCR: software for comprehensive adaptive immunity profiling. *Nat Methods*. 2015;12(5):380-381.
2. Minervina AA, Pogorelyy MV, Komech EA, et al. Primary and secondary anti-viral response captured by the dynamics and phenotype of individual T cell clones. *Elife*. 2020;9.
3. Minervina AA, Komech EA, Titov A, et al. Longitudinal high-throughput TCR repertoire profiling reveals the dynamics of T-cell memory formation after mild COVID-19 infection. *Elife*. 2021;10.
4. Schumann FL, Gross E, Bauer M, et al. Divergent Effects of EZH1 and EZH2 Protein Expression on the Prognosis of Patients with T-Cell Lymphomas. *Biomedicines*. 2021;9(12).
5. Bauer M, Vaxevanis C, Bethmann D, et al. Multiplex immunohistochemistry as a novel tool for the topographic assessment of the bone marrow stem cell niche. *Methods Enzymol*. 2020;635:67-79.
6. https://kpif.umbc.edu/image-processing-resources/imagej-fiji/determining-fluorescence-intensity-and-positive-signal/.
7. Herrera A, Cheng A, Mimitou EP, et al. Multimodal single-cell analysis of cutaneous T-cell lymphoma reveals distinct subclonal tissue-dependent signatures. *Blood*. 2021;138(16):1456-1464.
8. Integrated GEX and VDJ analysis of Connect generated library from human PBMCs. https://www.10xgenomics.com/resources/datasets/.
9. Hao Y, Stuart T, Kowalski MH, et al. Dictionary learning for integrative, multimodal and scalable single-cell analysis. *Nat Biotechnol*. 2024;42(2):293-304.

Supplementary Table 1: Characteristics of individual patients and samples.*

Pat. ID	Diagnosis	DOSC	Tissue	Age decade at diagnosis	Sex
001_1_1	AITL	ID	3	7	f
001_1_2	AITL	ID	1	7	f
002_1	T-LGLL	ID	1	8	m
003_1	AITL	ID	3	8	m
003_2	AITL	1st relapse/progression	1	8	m
003_3	AITL	2nd relapse/progression	1	8	m
003_4	AITL	3rd relapse/progression	1	8	m
004_1	AITL	ID	3	8	m
005_1	AITL	1st relapse/progression	3	7	m
006_1	AITL	ID	3	5	m
007_1	AITL	ID	3	8	m
008_1	AITL	ID	3	10	m
009_1	AITL	ID	3	8	m
010_1	AITL	ID	3	8	m
010_2	AITL	suspected relapse	3	8	m

010_3	AITL	relapse/progression	1	8	m
010_4	AITL	suspected relapse	1	8	m
011_1	AITL	ID	1	6	f
012_1	PTCL, NOS	ID	2	6	m
013_1	PTCL, NOS	ID	3	7	m
013_2	PTCL, NOS	1st relapse/progression	1	7	m
014_1	AITL	ID	3	6	f
014_2	AITL	1st relapse/progression	3	6	f
015_1	PTCL, NOS	1st relapse/progression	2	4	m
016_1	PTCL, NOS	ID	3	8	f
017_1	PTCL, NOS	1st relapse/progression	4	7	m
017_2	PTCL, NOS	2nd relapse/progression	4	7	m
018_1	PTCL, NOS	ID	3	6	f
019_1	ALCL	ID	10	6	m
020_1	T-PLL	ID	4	7	m
021_1	NKTCL	ID	5	4	m
022_1	NKTCL	ID	1	6	m
023_1	ALCL	ID	3	6	m
024_1	PTCL-TFH	ID	3	6	m
025_1	PTCL, NOS	ID	2	7	m
026_1	AITL	ID	3	7	m
027_1	PTCL, NOS	ID	3	7	m
028_1	SS	3rd relapse/progression	1	7	f
029_1	PTCL, NOS	ID	3	7	f
029_2_1	PTCL, NOS	1st relapse/progression	3	7	f
029_2_2	PTCL, NOS	1st relapse/progression	3	7	f
030_1	MEITL	ID	8	7	f
030_2	MEITL	1st relapse/progression	1	7	f
030_3	MEITL	1st relapse/progression	9	7	f
030_4_1	MEITL	1st relapse/progression	8	7	f
030_4_2	MEITL	1st relapse/progression	8	7	f
031_1_1	PTCL, NOS	ID	5	7	m
031_1_2	PTCL, NOS	ID	1	7	m
032_1	ALCL	ID	1	8	m
033_1	PTLD	ID	3	8	m
034_1	MF	ID	4	8	m
035_1	AITL	ID	3	8	m
035_2	AITL	1st relapse/progression	1	8	m

036_1_1	T-PLL	ID	3	8	f
036_1_2	T-PLL	ID	1	8	f
037_1	T-LGLL	ID	6	8	m
037_2	T-LGLL	1st relapse/progression	1	8	m
037_3	T-LGLL	2nd relapse/progression	1	8	m
038_1	AITL	ID	3	9	f
039_1	SS	1st relapse/progression	1	7	f
040_1	ALCL	ID	3	6	m
041_1	PTCL, NOS	ID	1	9	m
042_1	SPTCL	ID	2	6	m
043_1	ALCL	ID	3	6	f
044_1	PTCL, NOS	ID	3	6	f
045_1	AITL	ID	3	7	f
046_1	EATL	ID	8	5	m
047_1	ALCL	ID	1	6	m
048_1	AITL	ID	3	6	f
049_1	PTCL-TFH	ID	3	9	m
050_1	ALCL	ID	5	6	f
051_1	AITL	ID	1	6	f
052_1	PTCL, NOS	ID	1	5	m
053_1	PTCL, NOS	1st relapse/progression	4	6	f
054_1	PTCL-TFH	ID	3	6	m
055_1	T-PLL	ID	10	7	m
056_1	AITL	1st relapse/progression	10	4	m

*ID = initial diagnosis, DOSC = date of sample collection

Tissue code: 1 = bone marrow, 2 = connective tissue, 3 = lymph node, 4 = skin, 5 = nasopharynx, 6 = spleen, 8 = colon, 9 = peritoneum, 10 = Peripheral blood mononuclear cells (PBMC)

PTCL, NOS = peripheral T cell lymphoma, not otherwise specified

AITL = Angioimmunoblastic T cell lymphoma

ALCL = Anaplastic large cell lymphoma

NKTCL = Extranodal NK-/T-cell lymphoma, nasal type

PTCL-TFH = Peripheral T cell lymphoma, T follicular helper phenotype

MF = Mycosis fungoides

SS = Sézary Syndrom

T-PLL = T cell prolymphocytic leukemia

T-LGLL = T cell large granular lymphocytic leukemia

EATL = Enteropathy-associated T cell lymphoms

MEITL = Monomorphic epitheliotropic intestinal T cell lymphoma

PTLD = Post-transplant lymphoproliferative disorder

SPTCL = Subcutaneos panniculitis-like T cell lymphoma

Supplementary Table 2: QIAseq custom DNA panel, covered genes and regions.

chromosome	start	end	covered gene
chr1	120457925	120459275	NOTCH2
chr15	90631832	90631844	IDH2
chr15	90631928	90631940	IDH2
chr16	24135286	24135310	PRKCB
chr16	24166000	24166180	PRKCB
chr16	24183585	24183685	PRKCB
chr16	24185835	24185905	PRKCB
chr16	24192105	24192255	PRKCB
chr16	24196425	24196515	PRKCB
chr16	24196775	24196895	PRKCB
chr16	24202405	24202555	PRKCB
chr16	24231275	24231325	PRKCB
chr17	7572921	7573013	TP53
chr17	7573921	7574038	TP53
chr17	7576531	7576589	TP53
chr17	7576619	7576662	TP53
chr17	7576847	7576931	TP53
chr17	7577013	7577160	TP53
chr17	7577493	7577613	TP53
chr17	7578171	7578294	TP53
chr17	7578365	7578559	TP53
chr17	7579306	7579595	TP53
chr17	7579694	7579726	TP53
chr17	7579833	7579917	TP53
chr17	40354353	40354470	STAT5B
chr17	40354774	40354831	STAT5B
chr17	40359571	40359751	STAT5B
chr17	40362184	40362365	STAT5B
chr17	40474374	40475165	STAT3
chr19	6822246	6822327	VAV1
chr19	6828836	6828916	VAV1
chr19	6829624	6829802	VAV1
chr19	6832097	6832216	VAV1
chr19	6833190	6833301	VAV1
chr19	6833590	6833641	VAV1
chr19	6833718	6833749	VAV1

chr19	6833914	6833969	VAV1
chr19	6836438	6836584	VAV1
chr19	6853958	6854030	VAV1
chr19	17942030	17942215	JAK3
chr19	17942480	17942610	JAK3
chr19	17943325	17943520	JAK3
chr19	17943595	17943735	JAK3
chr19	17945375	17945535	JAK3
chr19	17945655	17945815	JAK3
chr19	17945885	17946030	JAK3
chr19	17946730	17946865	JAK3
chr19	17947935	17948025	JAK3
chr19	17948735	17948875	JAK3
chr19	17949065	17949200	JAK3
chr2	25457236	25457248	DNMT3A
chr2	74213525	74213838	TET3
chr2	74230231	74230298	TET3
chr2	74273399	74275543	TET3
chr2	74300670	74300771	TET3
chr2	74307619	74307723	TET3
chr2	74314951	74315170	TET3
chr2	74317018	74317179	TET3
chr2	74320023	74320123	TET3
chr2	74320650	74320798	TET3
chr2	74326397	74326744	TET3
chr2	74327514	74329308	TET3
chr20	39766418	39766430	LOC101927117;PLCG1
chr20	39792578	39792590	PLCG1
chr20	39794133	39794145	PLCG1
chr20	39802379	39802397	PLCG1
chr3	47058577	47058749	SETD2
chr3	47059122	47059234	SETD2
chr3	47061244	47061335	SETD2
chr3	47079150	47079272	SETD2
chr3	47084045	47084195	SETD2
chr3	47087971	47088116	SETD2
chr3	47098305	47098985	SETD2
chr3	47103647	47103841	SETD2
chr3	47108554	47108613	SETD2
chr3	47122451	47122578	SETD2
chr3	47125204	47125877	SETD2
chr3	47127679	47127809	SETD2
chr3	47129597	47129742	SETD2
chr3	47139439	47139576	SETD2
chr3	47142942	47143050	SETD2
chr3	47144830	47144918	SETD2

chr3	47147481	47147615	SETD2
chr3	47155360	47155499	SETD2
chr3	47158107	47158249	SETD2
chr3	47161666	47166043	SETD2
chr3	47168132	47168158	SETD2
chr3	47205338	47205419	SETD2
chr3	49412967	49412982	RHOA
chr3	176743280	176743317	TBL1XR1
chr3	176744155	176744267	TBL1XR1
chr3	176750753	176750929	TBL1XR1
chr3	176751980	176752118	TBL1XR1
chr3	176755880	176755965	TBL1XR1
chr3	176756095	176756227	TBL1XR1
chr3	176763911	176763982	TBL1XR1
chr3	176765082	176765190	TBL1XR1
chr3	176765268	176765342	TBL1XR1
chr3	176767779	176767931	TBL1XR1
chr3	176768260	176768403	TBL1XR1
chr3	176769286	176769519	TBL1XR1
chr3	176771555	176771711	TBL1XR1
chr3	176782702	176782770	TBL1XR1
chr3	176816248	176816334	TBL1XR1
chr3	176849145	176849167	TBL1XR1
chr4	106155094	106158602	TET2
chr4	106162490	106162591	TET2
chr4	106163985	106164089	TET2
chr4	106164721	106164940	TET2
chr4	106180770	106180931	TET2
chr4	106182910	106183010	TET2
chr4	106190761	106190909	TET2
chr4	106193715	106194080	TET2
chr4	106196199	106197681	TET2
chr6	138192359	138192664	TNFAIP3
chr6	138195976	138196177	TNFAIP3
chr6	138196819	138196977	TNFAIP3
chr6	138197127	138197308	TNFAIP3
chr6	138198207	138198398	TNFAIP3
chr6	138199563	138200493	TNFAIP3
chr6	138201202	138201394	TNFAIP3
chr6	138202166	138202461	TNFAIP3
chr9	21968222	21968246	C9orf53;CDKN2A
chr9	21968718	21968775	CDKN2A
chr9	21970895	21971212	CDKN2A
chr9	21974470	21974831	CDKN2A
chr9	21992445	21992484	CDKN2A
chr9	21994132	21994458	CDKN2A

chrX	41193500	41193555	DDX3X
chrX	41193702	41194027	DDX3X
chrX	41196655	41196723	DDX3X
chrX	41198283	41198341	DDX3X
chrX	41200731	41200874	DDX3X
chrX	41201742	41201911	DDX3X
chrX	41201984	41202094	DDX3X
chrX	41202463	41202609	DDX3X
chrX	41202984	41203080	DDX3X
chrX	41203277	41203386	DDX3X
chrX	41203486	41203657	DDX3X
chrX	41204427	41204582	DDX3X
chrX	41204651	41204806	DDX3X
chrX	41205476	41205668	DDX3X
chrX	41205752	41205880	DDX3X
chrX	41206106	41206270	DDX3X
chrX	41206559	41206709	DDX3X
chrX	41206887	41206977	DDX3X

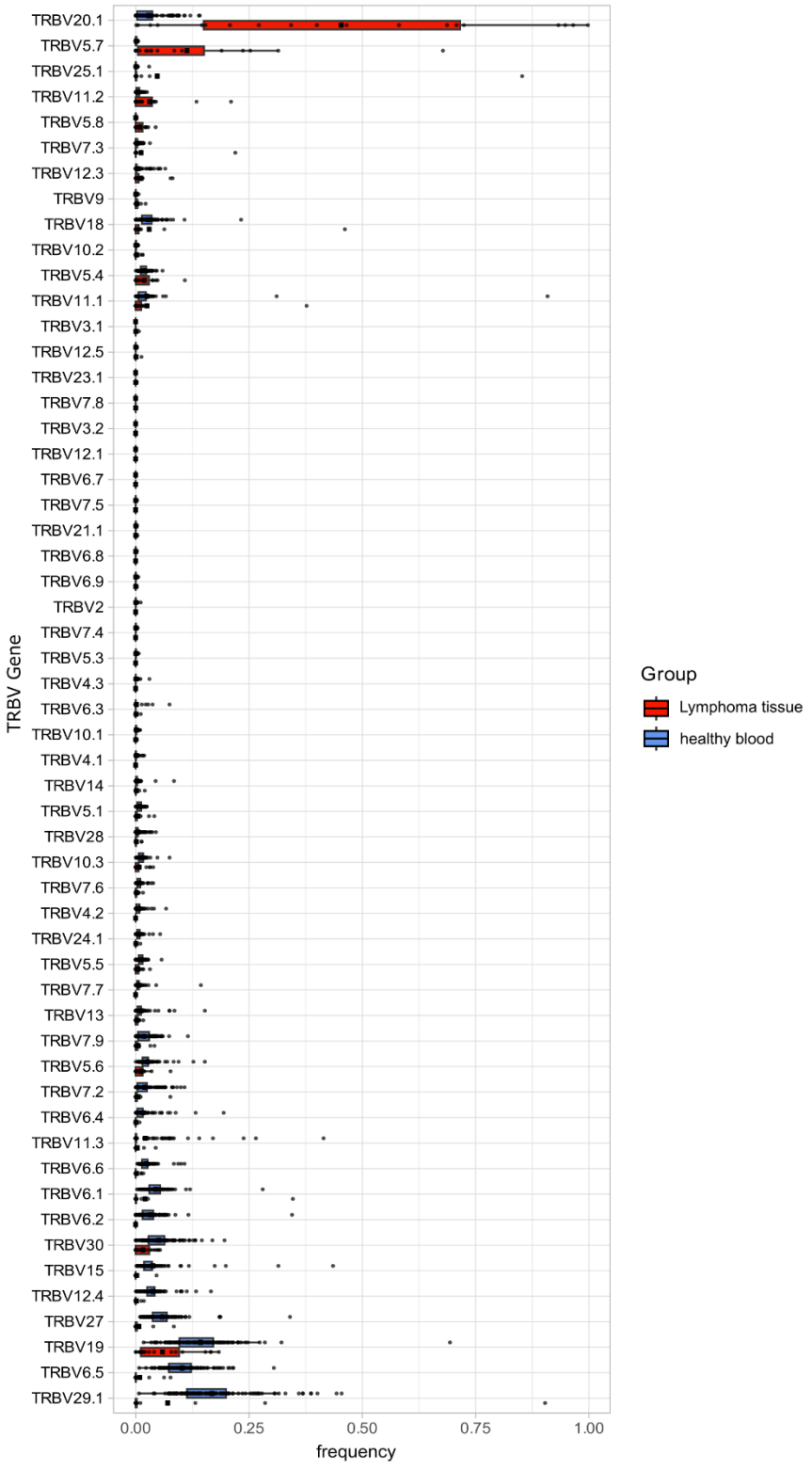

Supplementary Figure 1: TRBV gene usage and frequencies in all lymphoma samples (red, n=19) and healthy controls (blue, n=121). TRBV genes on the axis are sorted for their median group difference.

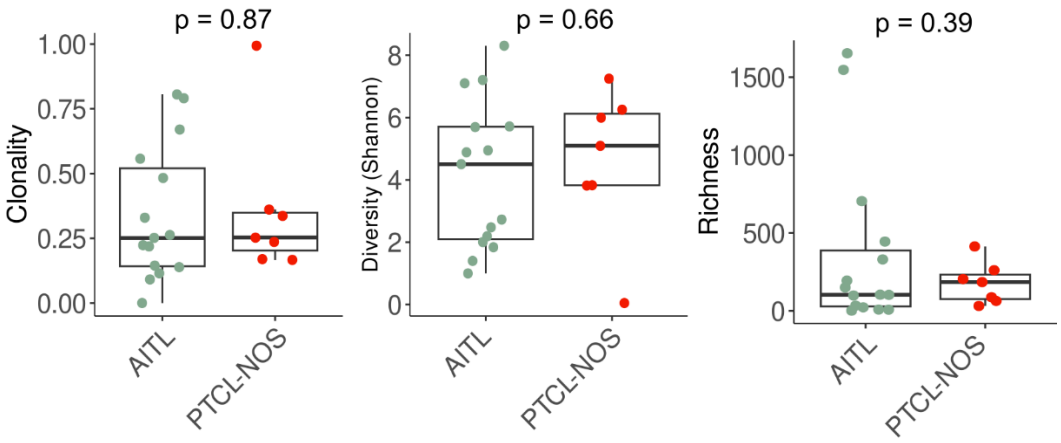

Supplementary Figure 2: TCR metrics in AITL (n=15) and PTCL NOS (n=7) lymphoma samples. Available samples at all time points are shown. Statistics: ANOVA

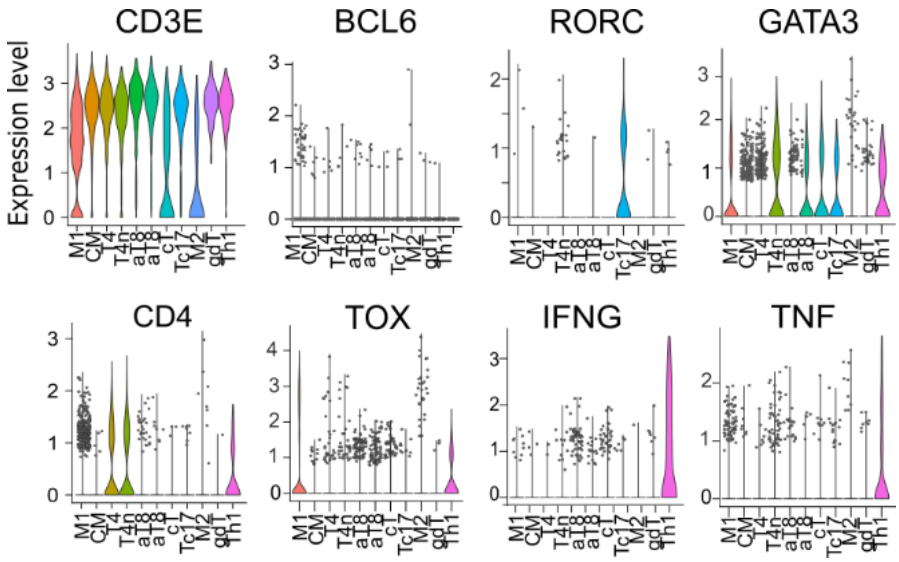

Supplementary Figure 3: Expression of canonical markers of T cell differentiation and function per cluster. Expression profiles in the integrated single cell dataset of T cells from two healthy and two lymphoma samples.

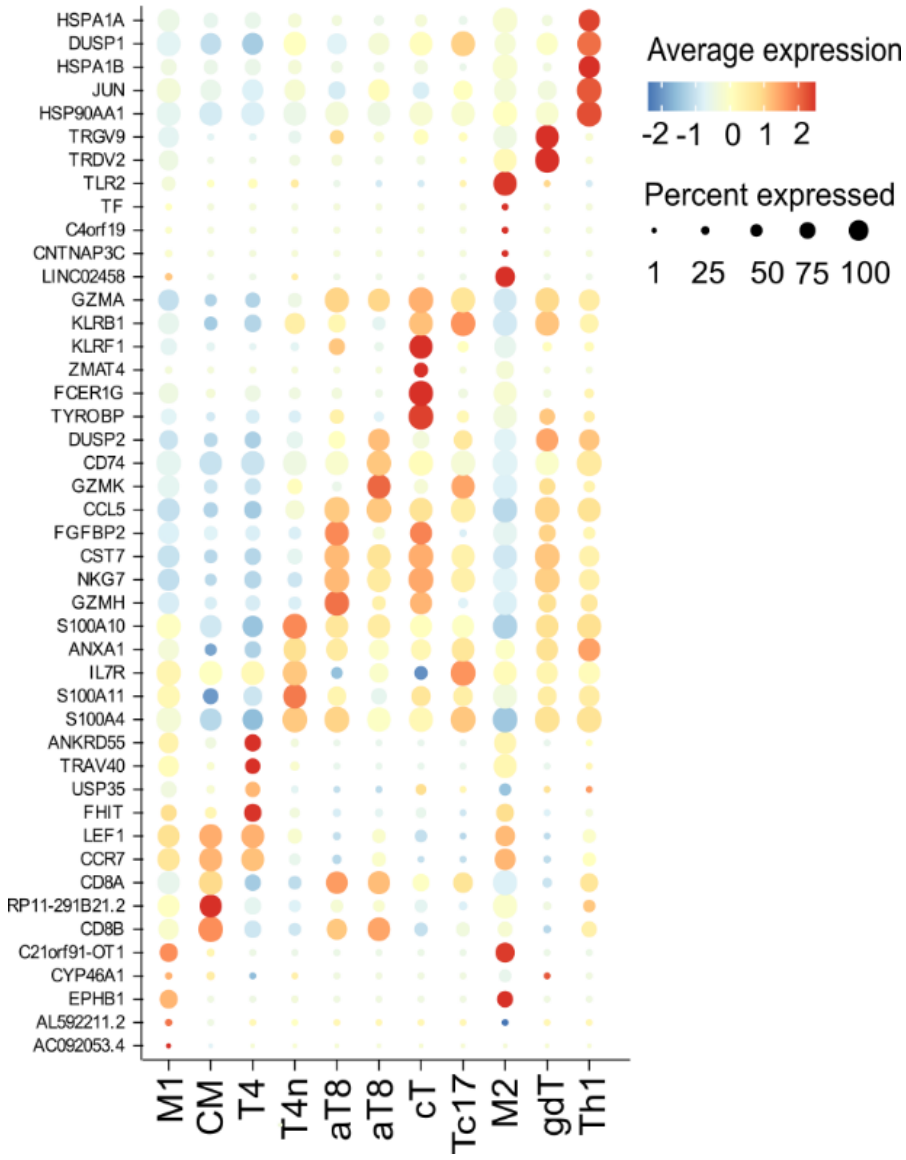

Supplementary Figure 4: Top five differentiating marker genes for each cluster from the integrated single cell analysis of T cells from two healthy and two lymphoma samples.

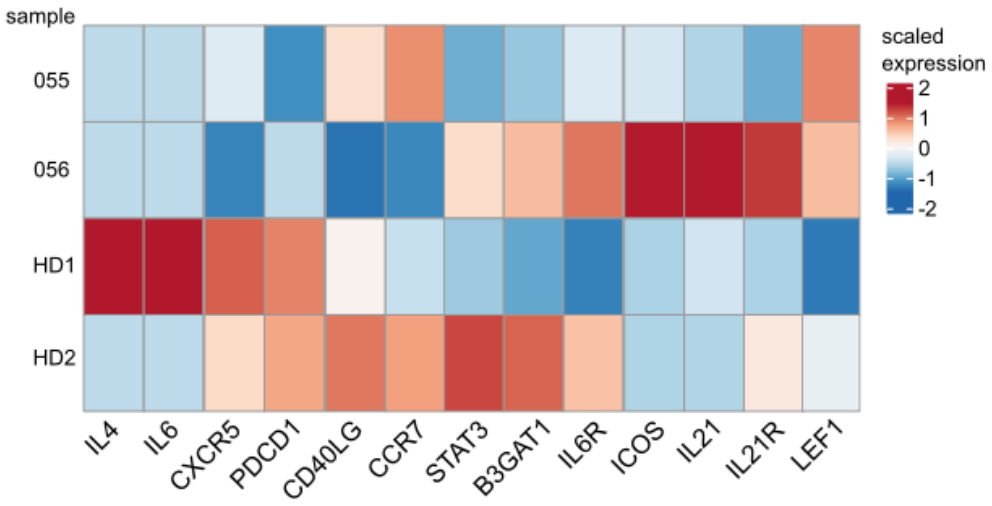

Supplementary Figure 5: Expression of markers associated with T follicular helper differentiation in single cell data, separated by samples.